Available online at www.sciencedirect.com
SCIENCE DIRECT®
Journal of Photochemistry and Photobiology A: Chemistry 165 (2004) 119–129
Journal of Photochemistry and Photobiology A:Chemistry
www.elsevier.com/locate/jphotochem

An experimental and theoretical investigation of the photocatalytic degradation of *meta*-cresol in TiO_2 suspensions: a model for the product distribution

Arzu Hatipoğlu, Nevim San, Zekiye Çınar*

Department of Chemistry, Yıldız Technical University, 34210 Istanbul, Turkey

Received 22 January 2004; accepted 1 March 2004

Abstract

The kinetics of the photocatalytic degradation of *meta*-cresol (*m*-CR) in the presence of TiO_2 has been investigated experimentally and theoretically. The effects of the catalyst loading and the initial concentration of *m*-CR on the degradation rate have been examined. A pseudo-first order kinetic model has been used to describe the results. A linear dependence of the rate constant upon the reciprocal of the initial *m*-CR concentration has been obtained. With the intention of predicting the primary intermediates and the product distribution, geometry optimizations of the reactants, the product radicals and the transition state complexes have been performed with the semiempirical PM3 method. The molecular orbital calculations have been carried out by an SCF method using RHF or UHF formalisms. Based on the results of the quantum mechanical calculations, the rate constants of the six possible reaction paths have been calculated by means of the transition state theory. Three predictors have been determined for the prediction of the most probable transition state and the reaction path. Branching ratio for each of the reaction paths has been calculated and the most probable intermediate has been determined to be 1,6-dihydroxy-3-methyl-cyclohexadienyl radical which then forms 3-methylcatechol. The results show that *m*-methylphenoxyl and *m*-hydroxybenzyl radicals which cause the formation of polyaromatics are not produced in the photodegradation of *m*-CR.

Keywords: Photocatalytic degradation; Photodegradation; Hydroxyl radicals; *m*-Cresol; PM3 method

1. Introduction

Due to its ability to generate OH radicals, heterogeneous photocatalysis is a promising new technique for water and air treatment [1–3]. The process is based on the combined use of low energy UV-A light and semiconductor photocatalysts of which the anatase form of TiO_2 is the most suitable [4,5]. Band gap excitation of TiO_2 generates electron–hole pairs that can initiate redox reactions on the surface of semiconductor particles. The oxidation reactions of adsorbed OH^- ions or H_2O molecules with the photogenerated holes yield OH radicals which are able to degrade a great variety of organic compounds [6].

Phenol derivatives are widely used chemicals in industry and in daily life. Due to their stability, bioaccumulation, solubility in water and high volatility, they constitute an important class of water and air contaminants. The reactions of these compounds with the OH radicals are the primary steps in their photodegradation mechanisms in both aqueous and gas phases. Although there are numerous investigations on the kinetics of the photocatalytic degradation reactions of phenolic compounds, the product distributions and the mechanisms of these reactions are still uncertain.

The photocatalytic degradation of phenol in aqueous TiO_2 suspensions have been studied by many investigators [6–10]. The results indicate that phenol decomposes completely to CO_2 and H_2O through a mechanism involving hydroxylation of the aromatic ring. Halogenated phenols are the most widely studied phenol derivatives [6,11–19]. It has been found out that the intermediates all correspond to the hydroxylation of the aromatic ring and the substitution of the –OH group occurs at the *para* and/or *ortho* sites with respect to the original phenolic functionality. Phenol derivatives with different substituents other than halogens are also of great concern not only because they cause severe health problems but they may also cause the formation of harmful products in their photocatalytic degradation reactions de-

* Corresponding author. Tel.: +90-212-449-1844; fax: +90-212-449-1514.
E-mail address: cinarz@yildiz.edu.tr (Z. Çınar).

1010-6030/$ – see front matter © 2004 Elsevier B.V. All rights reserved.
doi:10.1016/j.jphotochem.2004.03.008

pending upon the types of the substituents. However, there is very limited information on the kinetics and the reaction intermediates of the degradation reactions of such compounds [6,15].

In this study, *meta*-cresol (*m*-CR) was chosen as the representative member of this pollutant group because of its environmental importance, lack of data and its unusual structure. *m*-CR is toxic as are the other phenol derivatives. It is used as a disinfectant and an antioxidant. The major sources of *m*-CR are coal tar refining, petroleum refining, wood processing, and chemical manufacturing. Since it has a significant water solubility, 2.35 g/100 ml it is often present in wastewater discharges from such facilities. It may also be found in ground water wells and surface waters, where it has to be removed in order to achieve drinking water quality.

In this paper, we present the results of our investigation on the photocatalytic degradation kinetics of *m*-CR in aqueous TiO_2 suspensions. In the first part of the work, the effects of catalyst loading and the initial concentration of *m*-CR on the degradation rate were determined experimentally. In the theoretical part, with the intention of predicting the product distribution, quantum mechanical calculations were carried out for all the possible reaction paths.

2. Experimental details

2.1. Materials

The anatase form of TiO_2, Degussa P25 grade, with a particle size of 30 nm and a surface area of $50\,m^2\,g^{-1}$ was used as the photocatalyst without further treatment. All the chemicals that were used in the experiments were of laboratory reagent grade and used as received without further purification. The solutions were prepared with doubly distilled water.

2.2. Photoreactor

The experiments were carried out in a batch-type photoreactor. The reactor consists of two parts. The first part is the outside metallic cylinder which is 54.4 cm high and 31.6 cm in inside diameter. There are 5×8 W blacklight fluorescent lamps attached vertically onto the inner surface of the metallic cylinder at a distance of 12.0 cm apart from each other. At the bottom of the outer cylinder, there is a fan to cool the lamps. The second part of the reactor is a Pyrex glass cylinder which is 18.3 cm high and 9.0 cm in inside diameter with a volume of approximately 1000 ml and was used as the reaction vessel. The suspension was stirred magnetically throughout the reaction period in order to prevent TiO_2 particles from settlement. The incident light intensity was measured by means of a potassium ferrioxalate actinometer [20] and found to be 3.1×10^{-7} einsteins s^{-1}.

2.3. Experiments

In the experiments, a stock solution of *m*-CR at a concentration of $1.0 \times 10^{-2}\,mol\,l^{-1}$ was used. The suspension was prepared by mixing definite volumes of this solution containing the desired amount of *m*-CR with TiO_2. The suspension was agitated in an ultrasonic bath for 15 min in the dark before introducing into the photoreactor. The volume of the suspension was 600 ml. In the experiments, the amount of TiO_2 used was 0.3 g/100 ml which was determined as the optimum photocatalyst concentration. Owing to continuous cooling, the temperature of the reaction solution was $20 \pm 1\,^{\circ}C$. Under these conditions, the initial pH of the suspension was 5.8 ± 0.2 and measured by a pH-meter, Metrohm E-510.

All the samples, each 10 ml in volume were taken intermittently for analysis. The samples were then filtered through 0.45 μm Millipore discs. Before analyzing, all the solutions were wrapped with aluminium foil and kept in the dark. The concentration of *m*-CR was measured with a Unicam UV-Vis spectrophotometer. The calibration curves were prepared for a concentration range of $(1.0–10.0) \times 10^{-5}\,mol\,l^{-1}$ and the detection limit for *m*-CR was calculated to be $2.16 \times 10^{-5}\,mol\,l^{-1}$. In the experiments, the pH of the reaction solution decreased slightly. For 160 min of degradation, the change in the pH was 0.2–0.3 which did not affect the wavelength of maximum absorption in the UV-spectrum of *m*-CR.

3. Results and discussion

3.1. Kinetics of m-CR disappearance

Fig. 1 shows the kinetics of the disappearance of *m*-CR from an initial concentration of $1.5 \times 10^{-4}\,mol\,l^{-1}$ under three conditions. There was no observable loss of *m*-CR

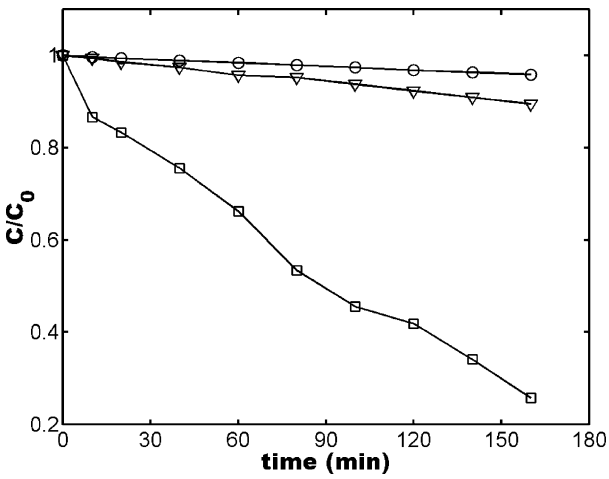

Fig. 1. Photocatalytic disappearance of *m*-CR ((○) with light, (▽) with TiO_2, (□) with light + TiO_2).

when the irradiation was carried out in the absence of TiO_2. In unirradiated suspensions, there was a slight loss approximately 6.4% due to adsorption onto TiO_2 particles. However, in the presence of TiO_2, a rapid degradation of *m*-CR occurred by irradiation. The concentration change amounts to 74.2% after irradiating for 160 min.

The semilogarithmic plots of concentration data gave a straight line. The correlation constant for the fitted line is 0.9928. This finding indicates that the photocatalytic degradation of *m*-CR in aqueous TiO_2 suspensions can be described by the first-order kinetic model, $\ln C = -kt + \ln C_0$, where C_0 is the initial concentration and C is the concentration of *m*-CR at time *t*. Under the experimental conditions used, the rate constant *k* for the degradation of *m*-CR was calculated to be $(7.85 \pm 0.33) \times 10^{-3}\,\mathrm{min}^{-1}$.

3.2. Effect of catalyst loading

Suspensions at pH $= 5.8 \pm 0.2$ and $1.5 \times 10^{-4}\,\mathrm{mol\,l}^{-1}$ *m*-CR concentration were used to study the effect of catalyst loading by varying the amount of TiO_2 from 0.1 to 0.5 g/100 ml. The effect of TiO_2 concentration on the degradation of *m*-CR is presented in Fig. 2 for two different irradiation times, 60 and 160 min. Both of the curves show that without catalyst, the degradation of *m*-CR is insignificant. As the concentration of TiO_2 increases, the rate of degradation increases upto a certain point, then begins to decrease slowly. Maximum degradation was obtained at a TiO_2 concentration of 0.3 g/100 ml. This observation indicates that beyond this optimum concentration, other factors affect the degradation of *m*-CR. At high TiO_2 concentrations, particles aggregate which reduces the interfacial area between the reaction solution and the catalyst, thus, they decrease the number of active sites on the surface. Light scattering by the particles and the increase in opacity may be other reasons for the decrease in the degradation rate.

Table 1
Effect of initial concentration of *m*-CR on the photocatalytic degradation rate

C_0 ($10^{-4}\,\mathrm{mol\,l}^{-1}$)	k ($\times 10^{-3}\,\mathrm{min}^{-1}$)	r
0.8	12.06 ± 0.37	0.9967
1.2	7.85 ± 0.33	0.9930
1.7	6.93 ± 0.25	0.9949
2.2	4.53 ± 0.15	0.9956
2.7	3.19 ± 0.51	0.9941

3.3. Effect of initial concentration of m-CR

Since the pollutant concentration is a very important parameter in water treatment, the effect of initial *m*-CR concentration was investigated over the concentration range $(0.8\text{–}2.7) \times 10^{-4}\,\mathrm{mol\,l}^{-1}$. Experimental results are presented in Table 1 and Fig. 3, together with the correlation coefficients *r* for each of the fitted lines. The results show that the degradation rate depends on the initial *m*-CR concentration. The rate constant *k* decreases with increase in the initial concentration of *m*-CR. This finding indicates that the degradation kinetics of *m*-CR is not of simple first order but pseudo-first order.

It was also observed from the slopes of the lines in Fig. 3 that the degradation rate constant decreases rapidly at low initial *m*-CR concentrations, then begins to change slowly as the initial concentration increases. As it can be seen from the values given in Table 1, the change in the rate constant is $1.34 \times 10^{-3}\,\mathrm{min}^{-1}$ when the initial *m*-CR concentration increases from 2.2×10^{-4} to $2.7 \times 10^{-4}\,\mathrm{mol\,l}^{-1}$. However, when the initial concentration increases from 0.8×10^{-4} to $1.2 \times 10^{-4}\,\mathrm{mol\,l}^{-1}$, the decrease in the rate constant is much greater, $4.21 \times 10^{-3}\,\mathrm{min}^{-1}$.

The reason for this initial concentration dependence of the photocatalytic degradation rate of *m*-CR may be attributed to the fact that the degradation reaction occurs on TiO_2 particles

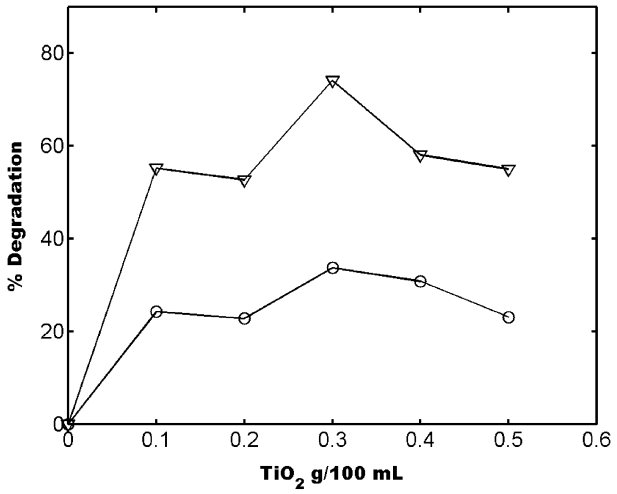

Fig. 2. Effect of TiO_2 loading on the photocatalytic degradation rate of *m*-CR, ((○) 60 min, (▽) 160 min).

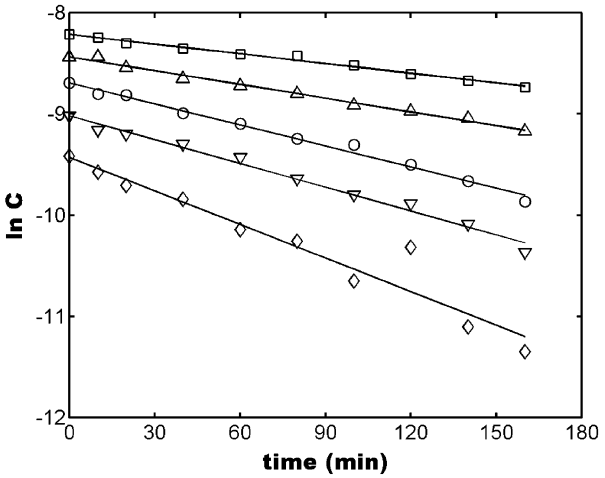

Fig. 3. Effect of initial concentration on the photocatalytic degradation rate of *m*-CR, ((□) $2.7 \times 10^{-4}\,\mathrm{mol\,l}^{-1}$, (△) $2.2 \times 10^{-4}\,\mathrm{mol\,l}^{-1}$, (○) $1.7 \times 10^{-4}\,\mathrm{mol\,l}^{-1}$, (▽) $1.2 \times 10^{-4}\,\mathrm{mol\,l}^{-1}$, (◇) $0.8 \times 10^{-4}\,\mathrm{mol\,l}^{-1}$).

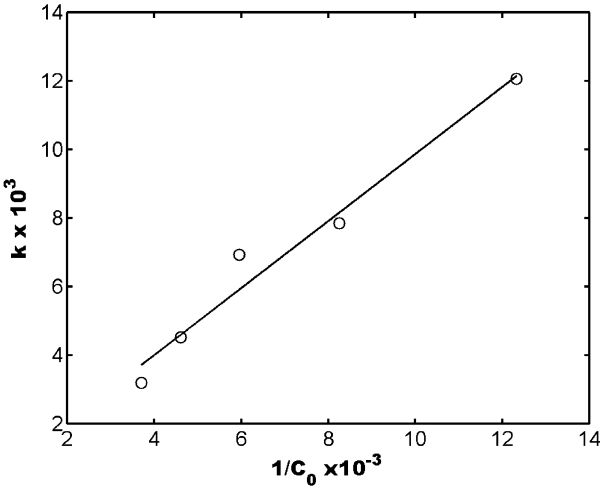

Fig. 4. Plot of the apparent rate constant vs. the reciprocal of the initial *m*-CR concentration.

as well as in solution [21]. On the photocatalyst surface, the reaction occurs between the OH radical generated at the active OH^- sites and a *m*-CR molecule from the solution. Thus, when the initial concentration is high, the number of these available active sites is decreased by *m*-CR molecules due to their competitive adsorption on TiO_2 particles and rate of transfer of *m*-CR from the solution does not affect the degradation rate. But, when the initial *m*-CR concentration is low, transfer rate plays an important role. The degradation rate constants obtained in this study are proportional to the reciprocal of the initial *m*-CR concentration (Fig. 4). The correlation constant for the fitted line is 0.9848.

3.4. Theoretical prediction of the primary intermediates

The photocatalytic degradation reactions of aromatic pollutants may take place through the formation of harmful intermediates such as polyaromatics, that are more toxic than the original compounds. Therefore, knowledge on the identities of the intermediates is a necessity in such processes. In aqueous TiO_2 suspensions, aromatic compounds are oxidized through two different mechanisms, either by hydroxylation of the aromatic ring [7,8,22] or by direct electron transfer to TiO_2 followed by the addition of a water molecule and loss of a proton [23–25]. While the two pathways are very different processes, they give similar product distributions. Therefore, the photocatalytic degradation of *m*-CR may be based on hydroxyl radical chemistry. In this study, in order to predict the primary intermediates, the kinetics of the reaction of *m*-CR with hydroxyl radicals has been investigated theoretically. The geometric parameters, the electronic and thermodynamic properties of the reactants, the product radicals and the transition state complexes have been calculated by quantum chemical methods. The rate constants over a range of temperatures for all the possible reaction paths have also been calculated. And finally, the product distribution for the degradation reaction of *m*-CR has been predicted.

3.4.1. Reaction paths

Hydroxyl radical is a very active species. It has a strong electrophilic character [26]. Once formed, the hydroxyl radical can readily attack the aromatic molecule and produce the reaction intermediates. The subsequent reactions of these intermediates lead to the mineralization of the compound.

OH radical reactions with aromatic compounds proceed by two reaction pathways; H-atom abstraction from C–H or O–H bonds and addition to aromatic rings. Six different reaction paths for the reaction of *m*-CR with the OH radical were determined by the nature of the substituent groups and the carbon atoms of the aromatic ring. The first four of the reaction paths, *o*1-addition, *o*2-addition, *m*-addition, *p*-addition shown in Fig. 5, are OH-addition reactions. The OH radical attacks a ring carbon with its unpaired electron and upon contact forms a C–O bond, while a π-bond of the aromatic system is broken and a hydroxycyclohexadienyl type radical (*o*1-R, *o*2-R, *m*-R, and *p*-R) is formed. The remaining two reaction paths H_o-abstraction and H_{Me}-abstraction are hydrogen abstractions from the functional –OH and $–CH_3$ groups producing a radical and a water molecule. The abstraction of hydrogen H_o from the –OH group produces *m*-methylphenoxyl (H_o–R) radical, whereas the abstraction of one of the methyl hydrogens H_{Me} yields *m*-hydroxybenzyl radical (H_{Me}–R). The process of H-abstraction by the OH radical is a simple atom-transfer reaction in which the bond to the hydrogen atom in –OH or $–CH_3$ is broken and a new bond to the oxygen atom of the OH radical is formed.

3.4.2. Method of calculation

Geometry optimizations of the reactants, the product radicals and the transition state complexes were performed with the semiempirical PM3 method within the MOPAC 6.0 package [27]. The molecular orbital calculations were carried out by a self-consistent field SCF method using the restricted RHF or unrestricted UHF Hartree-Fock formalisms depending upon the multiplicity of each species. The molecular models were created by using the mean bond distances and tetrahedral angles for sp^3 hybridized carbon and oxygen atoms. In the calculation of the hydroxylated radicals, the aromatic ring was left undisturbed and the attacking OH radical was assumed to form a tetrahedral angle with the C–H bond. These structures were input coordinates for PM3 calculations. The criterion for terminating all optimizations was increased by using the PRECISE option. The most stable conformers for the reactant *m*-CR molecule and the product radicals were determined by carrying out a conformer search [28,29].

Vibrational frequencies were calculated for the determination of the reactant and the product structures as stationary points and true minima on the potential energy surfaces. All possible stationary geometries located as minima were generated by free rotation around single bonds. All the station-

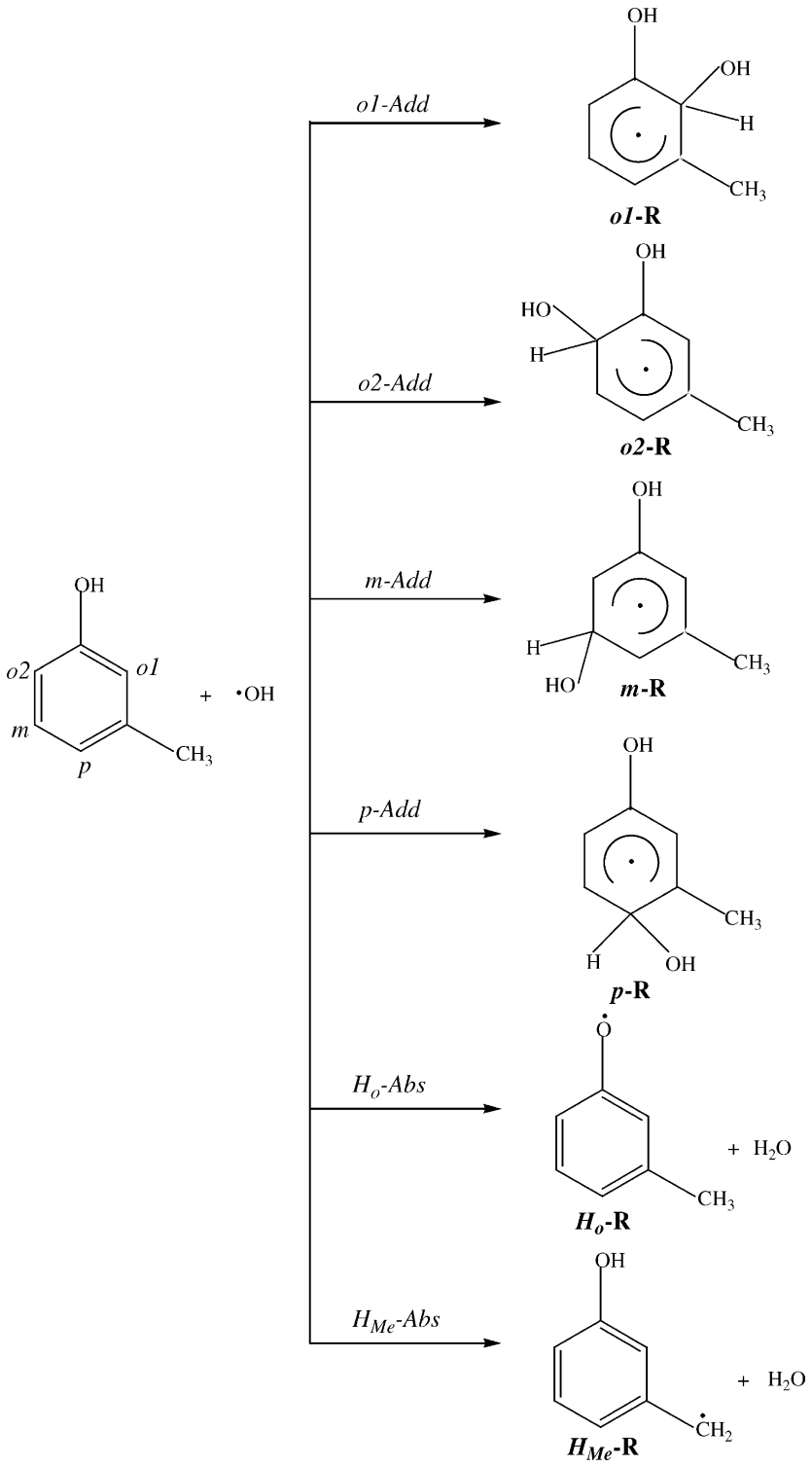

Fig. 5. Possible reaction paths for *m*-CR + OH reaction.

ary points were confirmed by the presence of positive vibrational frequencies. For a stationary point, the first derivatives of the energy with respect to changes in the geometry are zero. Whereas, the criterion for a minimum is that all eigenvalues of the Hessian matrix are positive [30]. The forming C–O bonds in the addition paths and the H–O bonds in the abstraction paths were chosen as the reaction coordinates in the determination of the transition states and each transition state was characterized with only one negative eingenvalue in its force constant matrix.

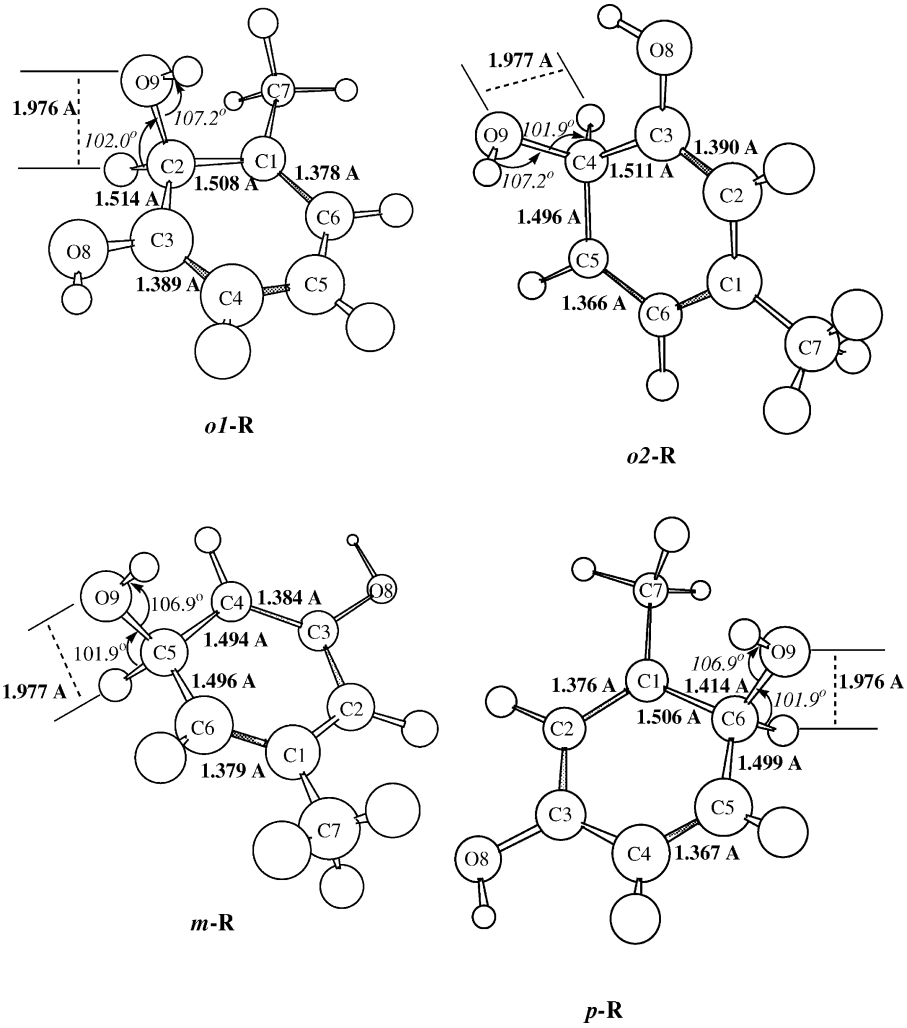

Fig. 6. The optimized structures of the radicals produced in the OH-addition paths.

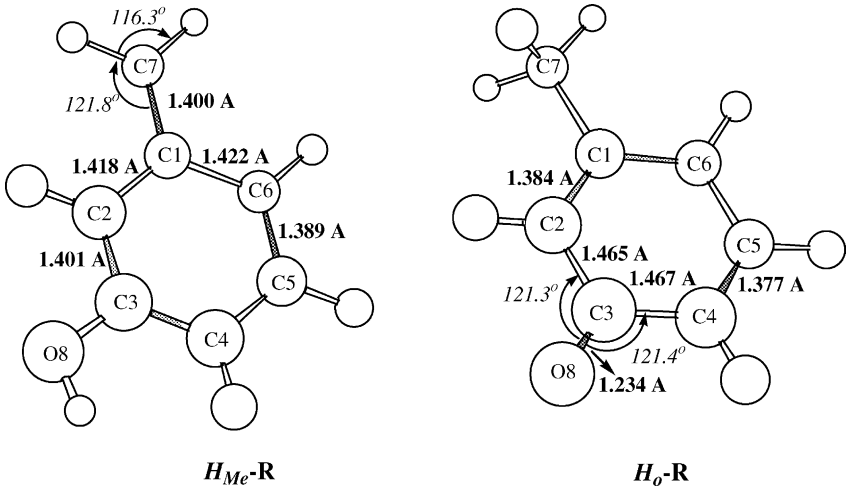

Fig. 7. The optimized structures of the radicals produced in the H-abstraction paths.

Table 2
Energetic parameters for the radicals

Radical	E (au)	ΔH_f (kcal mol^{-1})
*o*1-R	−57.149	−63.311
*o*2-R	−57.152	−65.256
m-R	−57.148	−62.495
p-R	−57.150	−63.500
H_o–R	−45.203	−6.190
H_{Me}–R	−45.202	−5.449

3.4.3. Product radicals

Six different radicals were determined as the products of the reaction between *m*-CR and the OH radical. The structures of all the radicals were fully optimized. Figs. 6 and 7 show the optimized structures of the forming radicals. The total energies E and the heats of formation ΔH_f obtained for each of the possible product radicals are presented in Table 2.

As can be seen from the values in Table 2, the radicals *o*1-R, *o*2-R, *m*-R, and *p*-R produced in the addition paths are more stable than the ones produced in the two abstraction paths H_o–R and H_{Me}–R. The reason may be attributed to the fact that all the radicals produced in the addition paths have hydrogen bond like stabilizations as shown in Fig. 6. The interaction distance between the original hydrogen atom at the addition center and the oxygen atom of the added OH was calculated to be around 1.977 Å for the four radicals. Among the four radicals produced in the addition paths, *o*2-R radical having the lowest E and ΔH_f is the most stable. *p*-R and *o*1-R radicals are 2 kcal mol^{-1} less stable, *m*-R 3 kcal mol^{-1}, H_o–R and H_{Me}–R radicals are around 60 kcal mol^{-1} less stable than the *o*2-R radical. By using the localization approach of Wheland's approximation [31] it may be predicted that the OH addition is the most probable reaction path and that the position of attack of the OH radical is the *ortho* (*o*2) position with respect to the phenolic –OH group.

3.4.4. Transition state structures

Six transition state complexes TS, one for each of the possible reaction paths were identified. The optimized structures of the transition states together with the necessary geometric parameters are presented in Figs. 8 and 9. In the addition

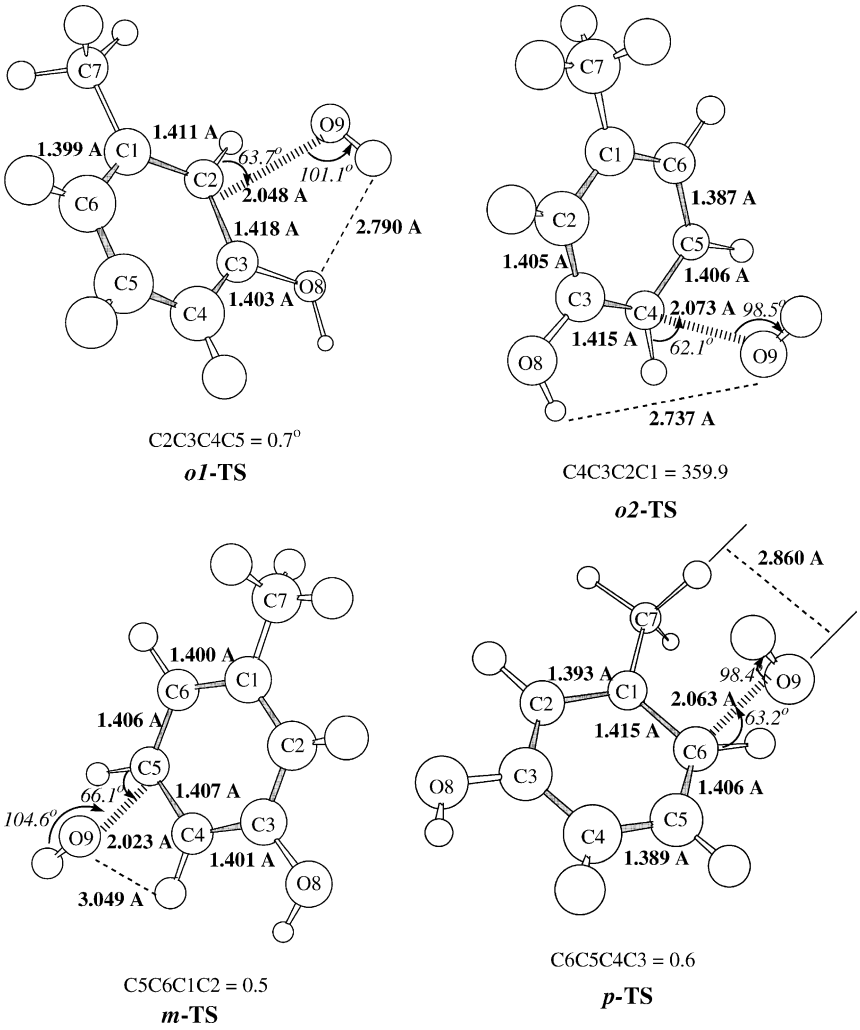

Fig. 8. The optimized structures of the transition states for OH-addition paths.

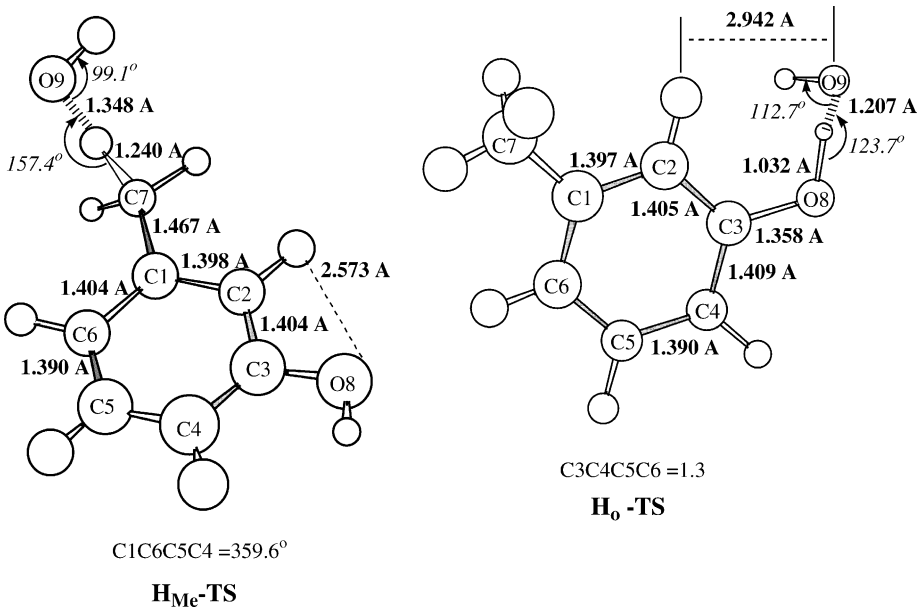

Fig. 9. The optimized structures of the transition states for H-abstraction paths.

paths, it was observed that the major structural changes relative to the parent *m*-CR molecule are all localized around the carbon atom to which the OH radical attacks. The two C–C bonds connecting to the addition center lengthen by 0.015–0.019 Å, whereas the change in the bond lengths of the subsequent C–C bonds is less, around ±0.004 Å. This finding indicates that the two C–C bonds connecting to the addition center have single, rather than double bond character. The ones away from the addition center have a more pronounced double bond character. The OH group is oriented such that the oxygen atom comes from the top of the ring making a 60° angle with the plane of the ring. In *m*-TS and *o*1-TS, the hydrogen atom points towards the exterior whereas in *p*-TS and *o*2-TS to the interior part of the ring. In the case of the *o*2-TS, the phenolic hydrogen rotates out of the ring plane by 10° to form a hydrogen bond to the adding oxygen. The interaction distance was calculated to be 2.737 Å. In the addition complexes, the hydrogen atom at the addition center also rotates by 6.7–8.2°. The angle between the forming C–O bond and the C–H bond is 62.1–66.1°.

In the abstraction complex H_o–TS, all the geometric changes are located around the phenolic group and the carbon atom connecting it. Since a new bond is being formed between the phenolic hydrogen and the oxygen atom of the OH radical, the C3–O8–H angle widens by 4.9°. There is also a slight elongation in the breaking bond, around 0.083 Å, which causes a shortening of the C3–O8 bond by 0.011 Å. Furthermore, it was also observed that the phenolic hydrogen rotates out of the ring plane by 11°. The OH group is oriented such that the oxygen atom comes from the top of the ring, making a 62.7° angle with the plane of the ring, while the hydrogen atom points towards the exterior part of the ring.

In the case of H_{Me}–TS, two major changes occur upon the approach of the OH radical to the *m*-CR molecule. One is the lengthening of the C7–H1 bond being broken and the other is the shortening of the C1–C7 bond. The lengthening of the C7–H1 bond is 0.142 Å, while the shortening is around 0.019 Å. It was also observed that the $–CH_3$ group rotates by 18° with respect to its original position in the *m*-CR molecule. As a result of the elongation of the C7–H1 bond being broken, the two H1–C7–H angles get narrower by 5.5°, while the other H–C7–H angle widens approximately by 3.4°. The C1–C7–H angles widen by 3.1– 4.0° as well.

From the analysis of the properties of the transition states, three predictors were determined for the prediction of the most probable TS and the reaction path; the length of the forming C–O or O–H bond *r*, its bond order *n* and the heat of formation ΔH_f of the TS. They are presented in Table 3. The forming bond length is a sensitive measure for the formation of the TS along the reaction coordinate. As it can be seen from the values given in Table 3, the addition complexes have much longer C–O bonds as compared to the C–O bonds in the corresponding radicals, 1.414 Å. This suggests that the addition complexes are early transition states and is in clear agreement with their small bond orders. Whereas, the

Table 3
The predictors for the determination of the most probable transition state

TS	*r* (Å)	*n*	ΔH_f (kcal mol^{-1})
*o*1-TS	2.048	0.165	−24.805
*o*2-TS	2.073	0.147	−26.411
m-TS	2.023	0.172	−22.557
p-TS	2.063	0.155	−25.252
H_o–TS	1.207	0.315	−14.055
H_{Me}–TS	1.348	0.345	−20.405

two abstraction complexes have much higher bond orders, indicating that they form late along the reaction coordinates. Among the four addition complexes, the longest C–O bond and the smallest bond order belong to *o*2-TS. Furthermore, *o*2-TS was found to have the lowest heat of formation among all the possible transition states indicating that it is the most thermodynamically stable one, followed by *p*-TS, *o*1-TS, and *m*-TS. H_o–TS and H_{Me}–TS are the least stable ones. Thus, we may conclude that *o*2-TS is the most probable transition state structure.

3.4.5. Energetics of the reaction paths

The activation energies for all the possible reaction paths were calculated as the difference between the heats of formation of the transition state complexes and the sum of the heats of formation of the reactants. The activation energies E_a and the heats of reaction ΔH_r calculated as the sum of the heats of formation of the products minus the sum of the heats of formation of the reactants are presented in Table 4.

The values in Table 4 show that the activation energies for the OH-addition paths are lower than the ones for the H-abstraction paths. The lowest activation energy belongs to path *o*2-addition for which the position of attack is at the *ortho*-carbon designated as *o*2 in Fig. 5. The energy barrier for *p*-addition path is 1.159 kcal mol^{-1}, for *o*1-addition 1.606 kcal mol^{-1} and for *m*-addition path 3.854 kcal mol^{-1} higher than the energy barrier for *o*2-addition path. The difference in the energy barriers for the addition paths can be explained by the features of the transition states. All the transition state complexes show hydrogen bond like stabilizations as shown in Fig. 8. The corresponding interaction distances are 2.737 Å for *o*2-TS, 2.790 Å for *o*1-TS, 2.860 Å for *p*-TS, and 3.049 Å for *m*-TS. The shorter interaction distances cause larger stabilizations and lower energy barriers. Thus, the longer interaction in the latest one causes an increase in the energy barrier. Moreover, *o*2-addition path was found to have the highest exothermicity. The result is consistent with Hammond's postulate [32] stating that early transition states have low energy barriers and high exothermicities. So, we may conclude that *o*2-TS is the most probable transition state in accordance with the two former predictions.

As for the abstraction paths, H_o-abstraction was found to have the highest activation energy, so H_o–TS is the least probable transition state. The energy barrier for

Table 4
Activation energies and heats of reaction ΔH_r for the reaction paths

Path	E_a (kcal mol^{-1})	ΔH_r (kcal mol^{-1})
*o*1-Addition	3.308	−35.198
*o*2-Addition	1.702	−37.143
m-Addition	5.556	−34.382
p-Addition	2.861	−35.739
H_o-abstraction	14.058	−31.488
H_{Me}-abstraction	7.708	−30.746

Table 5
Rate constants and branching ratios for the reaction paths

Path	k (cm^3 molecule^{-1} s^{-1})	Branching ratios
*o*1-Addition	1.594×10^{-14}	0.00021
*o*2-Addition	7.475×10^{-11}	0.99125
m-Addition	4.818×10^{-15}	0.00006
p-Addition	6.412×10^{-13}	0.00850
H_o-abstraction	1.088×10^{-19}	1.443×10^{-9}
H_{Me}-abstraction	5.281×10^{-18}	7.003×10^{-8}

H_{Me}-abstraction path is 6.347 kcal mol^{-1} less than the barrier for H_o-abstraction. The reason may again be attributed to the hydrogen bond like interactions. The corresponding interaction distances in H_o–TS and H_{Me}–TS are 2.942 and 2.573 Å, respectively. The shorter interaction distance in the latter one causes a larger stabilization, therefore, it shows a lower energy barrier.

3.4.6. Rate constants and product distribution

The rate constant k for each reaction path was calculated by using the transition state theory over a temperature range 200–400 K. The classical rate constant k in transition state theory is

$$k = \frac{k_B T}{h} \frac{q_{TS}}{q_{CR} q_{OH}} e^{-E_a/RT} \quad (1)$$

where k_B is Boltzmann's constant, T the temperature, h the Planck's constant, q's the molecular partition functions for TS and the reactant species, *m*-CR and $^{\bullet}$OH, and E_a is the activation energy. Each of the molecular partition functions was assumed to be the product of translational, rotational, vibrational, and electronic partition functions of the corresponding species. The calculated rate constants for 300 K are presented in Table 5.

As can be seen from the values given in Table 5, among all the possible reaction paths, the highest rate constant be-

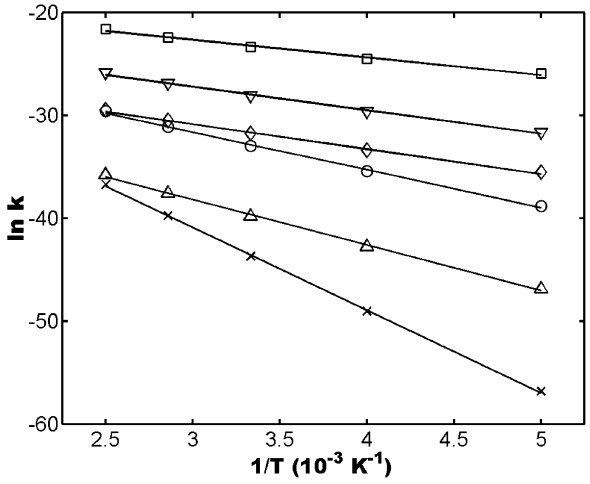

Fig. 10. Arrhenius plots for the possible reaction paths ((▽) *p*-addition, (○) *m*-addition, (□) *o*2-addition, (◇) *o*1-addition, (△) H_{Me}-abstraction, (×) H_o-abstraction).

Table 6
Product distribution for the reaction of *m*-CR with OH radicals

Path	Primary intermediate	Relative concentration (%)
*o*1-Addition	*o*1-R	0.02
*o*2-Addition	*o*2-R	99.13
m-Addition	*m*-R	0.00
p-Addition	*p*-R	0.85
H_o-abstraction	H_o–R	0.00
H_{Me}-abstraction	H_{Me}–R	0.00

longs to *o*2-addition. Whereas, H_o-abstraction was found to be the slowest reaction path in consistent with their energy barriers. Arrhenius plots in Fig. 10 also support these findings.

The branching ratio for each of the reaction paths was calculated by dividing the corresponding rate constant by the sum of the rate constants for all the possible reaction paths. The results presented in Table 5 show that the highest ratio belongs to *o*2-addition. By using the branching ratios, the relative concentrations of the primary intermediates were calculated and the product distribution for the reaction of *m*-CR with the OH radical is presented in Table 6.

The product distribution obtained in this study shows that the most probable primary intermediate that forms in the photocatalytic degradation of *m*-CR is 1,6-dihydroxy-3-methyl-cyclohexadienyl radical (*o*2-R) which then forms 3-methylcatechol. Since *m*-methylphenoxyl and *m*-hydroxybenzyl radicals were found to be the least probable ones, we may conclude that polyaromatic compounds do not form in the photocatalyic degradation of *m*-CR.

4. Conclusions

The principal conclusions of the present study can be summarized as follows:

1. The photocatalytic degradation of *m*-CR in aqueous TiO_2 suspensions follows a pseudo-first order kinetics.
2. The apparent rate constant depends on the initial *m*-CR concentration.
3. A linear dependence of the rate constant upon the reciprocal of the initial concentration has been obtained.
4. *o*2-R radical produced by the addition of OH to the *o*2-carbon is more stable than all the other product radicals.
5. Three predictors have been determined for the prediction of the most probable transition state and the reaction path; the length of the forming C–O or O–H bond, the bond order for this bond and the heat of formation of the TS.
6. The activation energies for the addition paths are lower than the ones for the abstraction paths.
7. *o*2-TS occurs early along the reaction coordinate giving rise to a long C–O bond and a small bond order. Thus, the lowest activation energy and the highest exothermicity belong to *o*2-addition path.
8. The highest rate constant belongs to *o*2-addition whereas H_o-abstraction has the slowest rate.
9. The most probable primary intermediate has been determined to be 1,6-dihydroxy-3-methyl-cyclohexadienyl radical which then forms 3-methylcatechol.
10. *m*-Methylphenoxyl and *m*-hydroxybenzyl radicals are the least probable intermediate products.

Acknowledgements

The authors express their thanks to A. Onur Çınar (Lehigh University, ATLSS, Bethlehem, PA, USA) for developing a special program for the determination of the transition state structures, to Yıldız Technical University Research Fund for financial support (Project no.: 20-01-02-03) and to Degussa Limited Company in Turkey for the generous gift of TiO_2.

References

[1] A. Mills, S. Le Hunte, J. Photochem. Photobiol. A 108 (1997) 1.
[2] D. Bahnemann, J. Cunningham, M.A. Fox, E. Pelizzetti, P. Pichat, N. Serpone, in: G.R. Helz, R.G. Zepp, D.G. Crosby (Eds.), Aquatic and Surface Photochemistry, Lewis, Baco Raton, FL, 1994, p. 261.
[3] P. Pichat, in: G. Ertl, H. Knözinger, J. Weitkamp (Eds.), Handbook of Heterogeneous Photo-Catalysis, vol. 4, VCH, Weinheim, 1997, p. 2111.
[4] D.F. Ollis, E. Pelizzetti, N. Serpone, Environ. Sci. Technol. 25 (9) (1991) 1523.
[5] D.W. Bahnemann, D. Bockelmann, R. Goslich, Sol. Energy Mater. 24 (1991) 564.
[6] A.M. Peiró, J.A. Ayllón, J. Peral, X. Doménech, Appl. Catal. B 30 (2001) 359.
[7] R.W. Matthews, S.R. McEvoy, J. Photochem. Photobiol. A 64 (1992) 231.
[8] Y.T. Wei, C. Wan, J. Photochem. Photobiol. A 69 (1992) 241.
[9] Y.T. Wei, Y.Y. Wang, C. Wan, J. Photochem. Photobiol. A 55 (1990) 115.
[10] A. Sclafani, L. Palmisano, E. Davi, J. Photochem. Photobiol. A 56 (1991) 113.
[11] J.C. D'Oliveira, C. Minero, E. Pelizzetti, P. Pichat, J. Photochem. Photobiol. A 72 (1993) 261.
[12] J.C. D'Oliveira, G. Al-Sayyed, P. Pichat, Environ. Sci. Technol. 24 (1990) 990.
[13] U. Stafford, K.A. Gray, P. Kamat, J. Catal. 167 (1997) 25.
[14] T. Pandiyan, O.M. Rivas, J.O. Martinez, G.B. Amezcua, M.A. Martinez-Carrillo, J. Photochem. Photobiol. A 146 (2002) 149.
[15] K.H. Wang, Y.H. Hsieh, M.Y. Chou, C.Y. Chang, Appl. Catal. B 21 (1999) 1.
[16] Y. Ku, L. Ren-Ming, L. Kuen-Chyr, Water Res. 30 (1996) 2569.
[17] W.F. Jardim, S.G. Moraes, M.M.K. Takiyama, Water Res. 31 (1997) 1728.
[18] J.N. Chen, Y.C. Chan, M.C. Lu, Water Sci. Technol. 39 (1999) 225.
[19] Y.C. Chan, J.N. Chen, M.C. Lu, Chemosphere 45 (2001) 29.
[20] J.G. Calvert, J.N. Pitts, Photochemistry, Wiley, New York, 1966, pp. 783–786.
[21] H. Al-Ekabi, P. De Mayo, J. Phys. Chem. 90 (1986) 4075.
[22] S. Das, M. Muneer, K.R. Gopidas, J. Photochem. Photobiol. A 77 (1992) 83.
[23] R.B. Draper, M.A. Fox, Langmuir 6 (1990) 1396.
[24] G. Lu, A. Linsebigler, J.T. Yates Jr., J. Phys. Chem. 99 (1995) 7626.
[25] L. Cermenati, P. Pichat, C. Guillard, A. Albini, J. Phys. Chem. B 101 (1997) 2650.

[26] V. Brezova, M. Ceppan, E. Brandsteterova, M. Breza, L. Lapcik, J. Photochem. Photobiol. A 59 (1991) 385.
[27] J.P. Stewart, MOPAC QCPE Program, 455, Bloomington Ind., 1990.
[28] J.P. Stewart, J. Comput. Chem. 10 (1989) 209.
[29] J.P. Stewart, J. Comput. Chem. 10 (1989) 221.
[30] M.W. Jurema, G.C. Shields, J. Comput. Chem. 14 (1) (1973) 89.
[31] M.K. Eberhardt, M. Yoshida, J. Phys. Chem. 77 (1973) 589.
[32] W.J. Hehre, L. Radom, P.R. Schleyer, J.A. Pople, Ab Initio Molecular Orbital Theory, Wiley, New York, 1986.